C-band disk-loaded-type accelerating structure for a high acceleration gradient and high-repetition-rate operation

T. Sakurai,[1,2,*] H. Ego,[2] T. Inagaki,[1] T. Asaka,[1,2] D. Suzuki,[3] S. Miura,[3] and Y. Otake[1]

[1]*RIKEN SPring-8 Center, Kouto 1-1-1, Sayo, Hyogo 679-5148, Japan*
[2]*Japan Synchrotron Radiation Research Institute (JASRI), Kouto, 1-1-1, Sayo, Hyogo 679-5198, Japan*
[3]*Mitsubishi Heavy Industries Mechatronics Systems Ltd., Komatsu-dori 5-1-16, Hyogo-ku, Kobe, Hyogo 652-0868, Japan*

(Received 13 January 2016; revised manuscript received 8 August 2016; published 19 April 2017)

A high-acceleration-gradient linear accelerator (LINAC) for an x-ray free electron laser (XFEL) offers the advantages of a short accelerator length and low construction costs. In addition, the high pulse repetition rate of the LINAC, which can drive multiple x-ray beam lines, provides additional user opportunities for experiments involving XFEL. A *C*-band disk-loaded-type accelerating structure was developed to achieve a high acceleration gradient of >50 MV/m and an rf-pulse repetition rate of 120 pps, which is twice as high as that of the XFEL facility, SACLA (60 pps). The structure has a quasiconstant gradient and a traveling wave type with an accelerating mode of TM01 − 2π/3. To reduce the surface electric fields, we employed a cross section with an ellipsoidal curvature around an iris aperture. The accelerating structure was manufactured for SACLA. High-power rf conditioning was conducted to investigate its performance. Owing to the conditioning, the acceleration gradient reached a value of more than 50.1 MV/m. The structure was operated without any serious issues at a repetition rate of 120 pps. The accelerating structures were installed in the dedicated accelerator for EUV-FEL at SACLA beam line-1. Finally, we obtained accelerated electron beams with the structures operated at an acceleration gradient of 41.4 MV/m.

I. INTRODUCTION

An x-ray free electron laser (XFEL), which can provide light with high peak brightness, femtosecond-region short pulse, and high spatial coherence, outperforms existing synchrotron radiation sources. The linac coherent light source (LCLS) and SPring-8 Angstrom compact free electron laser (SACLA) are operated to make an x-ray laser available to experimental users [1,2]. Following the establishment of LCLS and SACLA, many XFEL facilities have been constructed and commissioned around the world [3–5].

There are two important considerations, when constructing an XFEL facility. First, we should obtain the target electron energy with the acceleration length being as short as possible. This reduces the construction costs of the accelerator and its building. Therefore, it is necessary to use high-gradient accelerating structures. However, a high acceleration gradient is usually accompanied by an increase in surface electric fields in the structure. This phenomenon might increase the probability of electric discharges. Furthermore, it increases the dark current, which occurs

from the inner surface of the structure. The dark current causes demagnetization of the permanent magnets used in the undulator [6]. Hence, it is imperative to reduce the surface electric fields.

The acceleration gradient, E_{acc}, per unit length of a constant-gradient (CG) traveling-wave-type (TW-type) rf structure is calculated by

$$E_{acc} = \sqrt{\frac{P_{in} \cdot R_{sh} \cdot (1 - e^{-2\tau})}{L}}, \qquad (1)$$

where P_{in} is the input rf power, R_{sh} is the shunt impedance per unit length, τ is the attenuation constant, and L is the length of the structure [7]. Further, R_{sh} varies as a function of $f^{0.5}$, where f is the operation frequency of the structure. If the inner shape of the accelerating structure and the accelerating mode are fixed, and P_{in}, τ and L are constant parameters, then E_{acc} is proportional to $f^{0.25}$. The use of high frequencies reduces the filling time of the accelerating structure in proportion to $f^{-1.5}$; the stored energy is proportional to f^{-2} of the accelerating structure. To reduce the accelerator length, an accelerating structure with a high acceleration gradient field should be operated at as high a frequency as possible owing to the above-mentioned frequency-proportional relation.

Next we should consider sharing the beam time with many experimental users. This is because an XFEL facility is a light source that uses a linear accelerator (LINAC) that

can generate a high-quality electron beam. However, unlike a ring photon source, it is not easy for a LINAC-based light source to have many beam lines. An electron beam distribution technique from the LINAC to multiple beam lines is crucial to increase opportunities for user experiments. Multi-beam-line operation using a fast switching magnet is under development at several XFEL facilities [3–5,8,9]. However, the pulse rate of the x-ray laser per beam line inevitably decreases in the case of multi-beam-line operation. In SACLA, five beam lines can be constructed in future expansions. In this case, the x-ray laser repetition rate per beam line decreases to one-fifth of the present 60 pps accelerator repetition. To maintain a sufficient repetition rate for each beam line, the accelerator should be operated with a higher pulse repetition rate. In this case, an accelerating structure with a higher acceleration gradient and a higher pulse repetition rate contributes significantly toward increasing opportunities for user experiments while reducing the construction costs of the LINAC. To realize a higher acceleration gradient and a higher rf-pulse repetition rate, a C-band accelerator is one of the most promising solutions because of the already established technique.

A C-band accelerating structure was initially developed for a linear collider project at KEK [10]. The structure was first used on a large scale at SACLA. Since 2011, 128 columns of the structure have been operated in the acceleration gradient range of 35–38 MV/m at a maximum repetition rate of 60 pps [11]. In the KEKB project, a C-band disk-loaded-type accelerating structure with twice the energy gain of the existing S-band accelerating structure was designed, and it was operated at an acceleration gradient of 45 MV/m in the KEK injector linac [12]. In recent years, many C-band accelerating structures have been developed at several accelerator facilities around the world [13–15]. However, even though the rf breakdown rate of a high-gradient accelerating structure, which is proportional to the increase in its surface electric and magnetic fields, generally restricts its operation condition, the high-gradient behaviors of C-band accelerating structures, as shown by the experimental results obtained at some institutes [16–18], have not been investigated systematically.

For the above-mentioned reasons as well as to clarify the high-gradient characteristics of the accelerating structure, we have developed a new C-band accelerating structure that yields a high acceleration gradient (>50 MV/m), which is higher than that of practically operating linacs. Furthermore, we aim to realize operation with a repetition rate of 120 pps, which is twice as high as that of SACLA and the same as that of LCLS. Toward this end as mentioned above, we have developed a new accelerating structure with reduced surface electric fields and lower heat loads at higher repetition rates. This paper describes the design of the new C-band accelerating structure as well as the practical performance obtained in our experiments.

II. DESIGN OF THE ACCELERATING STRUCTURE

With regard to the design boundary of the C-band accelerating structure, the total length, filling time, and attenuation constant of the accelerating structure are key parameters, which should be the same as those of the existing choke-mode-type accelerating structure used in SACLA. This is because the existing accelerating structure of SACLA can be easily replaced with a new one, if any problem occurs in the future. The new C-band accelerating structure was designed on basis of the following criteria.

1. To obtain a high acceleration gradient of the accelerating structure using the present C-band rf sources, we choose an rf design parameter with high shunt impedance. Considering the above-mentioned boundary condition, we aim to obtain a shunt impedance of >60 MΩ/m using a copper rf cavity.

2. The increase in surface electric fields on a cell wall in the structure leads to an increase in the breakdown rate and dark current in the accelerating structure. The axial acceleration gradient is increased by 20% owing to the increase in the shunt impedance compared with the SACLA structure, while the surface electric field should be the same owing to the special cavity design.

3. The accelerating structure high-gradient behaviors governed by an rf-pulse heating [17,18] should be confirmed.

4. The heat load of the accelerating structure at 120-pps operation is twice as high as that of the existing 60 pps operation at SACLA. The cooling capacity of the water channels of the structure must be able to deal with this heat load.

To satisfy the above-mentioned criteria, we designed a C-band accelerating structure having the cross-sectional and outer views shown in Fig. 1. Table I lists the designed and measured parameters of the C-band accelerating structure. The material of the accelerating structure was copper. The designed structure is a disk-loaded and quasi-constant-gradient (CG) type. The longitudinal phase advance per unit cell of the structure is $2\pi/3$ radian in the TM01 transverse mode. The shunt impedance of the accelerating structure is maximized in the longitudinal $2\pi/3$ mode [7]. Because the geometric cell shape of this designed CG structure is simple compared to other wakefield damping structures, such as the waveguide-attached damping structure [19] and the choke-mode structure [10], it is expected to reduce the production costs. Furthermore, it is possible to perform precise phase adjustments by the dimpling method on the cell walls after vacuum brazing [20].

Various methods have been proposed for reducing the surface electric fields [21]. To reduce the surface electric fields on the cell walls in the structure, we introduced a cross section with an ellipsoidal curvature around an iris [17]. The maximum surface electric field, which depends on the axis ratio of the major (B) to the minor (A) semiaxis of the ellipse iris, was estimated. Figure 2
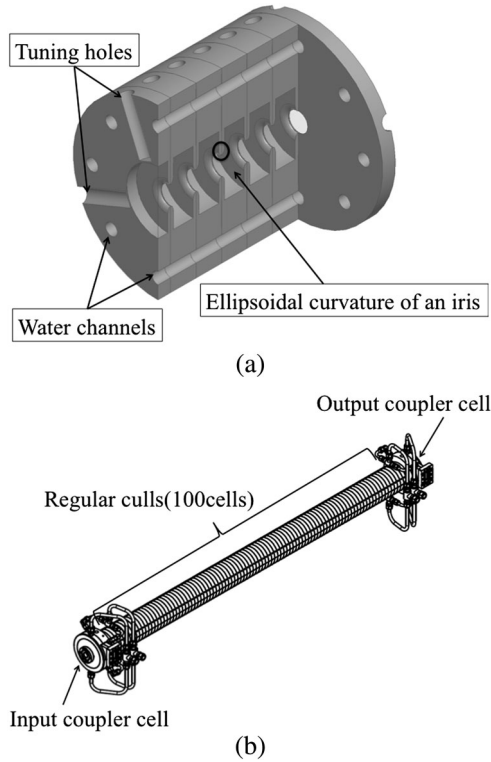
FIG. 1. (a) Cross-sectional view of the C-band disk-loaded-type accelerating structure. (b) Outer view of the new C-band accelerating structure.

shows a cross-sectional view of the ellipsoidal iris shape and the ratio (E_p/E_{acc}) of the maximum surface electric field, E_p, to the average acceleration field, E_{acc}, as a function of the ratio of B/A. The solid line with solid circle dots and the dashed line with open triangles in Fig. 2 denote E_p/E_{acc}s in the cases of the uppermost (n = 1) and the lowermost (n = 100) cells of the accelerating structure, respectively. At $B/A = 2.0$, the E_p/E_{acc} values of the uppermost and lowermost cells are 2.81 and 2.57, respectively. These values are lower than those of the circular curvature case ($B/A = 1.0$; E_p/E_{acc}s of the uppermost and the lowermost cells are 3.33 and 2.77). These results nearly satisfy the above-mentioned target value. Therefore, we chose $B/A = 2.0$. According to these cavity designs, the average shunt impedance of the new structure becomes 66 MΩ/m.

Furthermore, the possibility of breakdown and surface damage due to an rf-pulse heating was considered. The increase in temperature of the inner surface owing to the pulse heating is calculated as follows [17,18];

$$\Delta T = \frac{|H_t|^2}{\sigma\delta}\sqrt{\frac{t}{\pi\rho c_\varepsilon k}}, \tag{2}$$

where H_t is the surface magnetic field, t is the length of the rf pulse, σ is the electric conductivity, δ is the skin depth, ρ is the density of the accelerating structure material, C_ε is the specific heat capacity of the material, and k is the thermal conductivity of the material [18,22]. When the acceleration gradient and the length of the rf pulse are 50 MV/m and 0.3 μs, the surface magnetic fields at the axis ratios of $B/A = 1.0$ and 2.0 in the ellipsoidal iris are 0.11 and 0.10 MA/m, respectively. From Eq. (2), the increase in temperature, ΔT, is 6.2 and 4.7 K, respectively. These values are significantly lower than the breakdown limit described in [18,22], and we assume that such rf-pulse heating does not cause any breakdown or surface damage.

TABLE I. Design parameters and measured values of the C-band disk-loaded-type accelerating structure.

|		Design parameters	Measurements
Structure type		Quasiconstant gradient, traveling-wave-type	
Coupler type		J-type dual feed	
Resonant mode		TM01 − 2π/3	
Number of cells	N	100 regular cells	
		+2 coupler	
Iris diameter [mm]	$2a$	15.938	
		~12.107	
Cell diameter [mm]	$2b$	43.196	
		~41.869	
Disk spacing [mm]	d	17.495	
Disk thickness [mm]	t	4	
Cross-sectional shape of iris		Ellipsoidal curvature	
Effective length of acceleration [m]	L	1.767	
Operation frequency [MHz]	f	5712	5712
Average unloaded quality factor	Q_0	9300	8900
Average group velocity	v_g/c	0.023	0.022
Filling time [ns]	t_F	290	271
Attenuation constant	τ	0.59	0.54
Average shunt impedance [MΩ/m]	R_{sh}	66	64

(a)

(b)
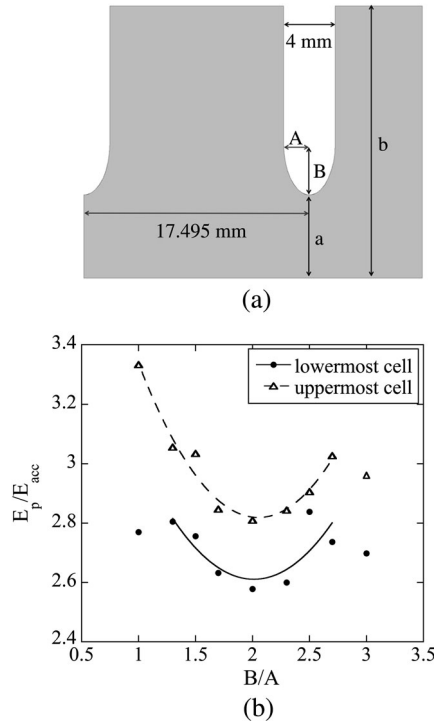
FIG. 2. (a) Cross-sectional view of the ellipsoidal curved iris. (b) Simulation result of the maximum surface electrical field over E_p/E_{acc} depending on the ratio of B/A. The circle and triangle markers show the ratios at the uppermost (n = 1) and lowermost (n = 100) cell cases, respectively. The solid curve is the quadratic regression curve excluding the points of B/A = 1.0, 3.0, and the dashed curve is the quadratic regression curve excluding the point of B/A = 3.0.

We designed the resonant frequency of the cavity cell to be 5712 MHz at a cavity temperature of 30 °C. In SACLA, the allowed rf phase jitter of the *C*-band main accelerator is less than ±0.5° [23]. An increase in the heat load of the accelerating structure causes thermal expansion of the cell and shifts the cell's resonant frequency. Consequently, the average temperature and frequency stability of the accelerating structure should have values within ± 0.11 K and ± 5.43 kHz, respectively, which are determined by the rf phase tolerance of ± 0.5°. To realize values within ± 0.11 K, we carefully designed a water-cooling method for the structure to effectively transfer the heat and to mitigate both the thermal expansion and the frequency shift of the cell. To estimate the frequency shift, the temperature distribution of the accelerating cell and the thermal and dimensional expansion were simulated using ANSYS [24]. Our simulated thermal design predicts the average heat load of the accelerating structure up to 3.8 kW at 120 pps operation. This value is equivalent to the heat loss when an input rf power of 80 MW is fed into the accelerating structure. We placed eight water channels having an inner diameter of 8 mm. The water flow rate per channel required by the design is 2.5 L/min for realizing the above-mentioned power dissipation. The counterflow method is
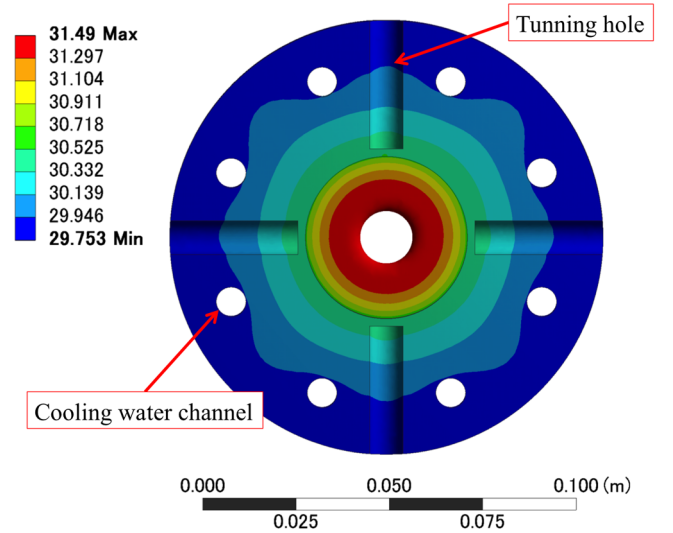

FIG. 3. Estimated temperature distribution of one accelerating cell with a cooling-water temperature of 27.6 °C at 120 pps operation. The rf power to be inputted to the accelerating structure is 80 MW.

adopted to minimize the temperature gradient along the accelerating structure.

Figure 3 shows the simulated temperature distribution of the accelerating cell at an average structure body temperature of 30 °C as the designed operating point, with operation repetition rate of 120 pps and a resonant frequency of 5712 MHz. In this case, the channel water flow rate is 2.5 L/min and the input rf power is 80 MW, corresponding to a heat load of 3.8 kW on the structure. The temperature of the cooling water at an inlet is 27.6 °C so that the temperature can be maintained at 30 °C. Thus the maximum temperature on the cell surface is 31.5 °C. The diameter of the cell (2*b*) increases by around 0.15 μm, which corresponds to a frequency of 20 kHz lower shifted from 5712 MHz. Furthermore, the required temperature stability of the structure is ±0.11 K as mentioned previously. To maintain the cavity resonant frequency of 5712 MHz at 30 °C within ±0.11 K for any rf-pulse repetition rate, we employ a precise temperature regulation system using the proportional integral differential feedback control method, which controls the electric power fed into a heater having a capacity of 7.7 kW [25]. This system also compensates the lower frequency shift by maintaining the temperature at 30 °C.

III. NINE-CELL TEST CAVITY

A. Fabrication

We fabricated nine-cell test cavities to check the designed rf property of the accelerating structure. The test cavities were checked on the basis of the following points: (i) Check the fabrication method and the surface roughness of the ellipsoidal curvature on the basis of the
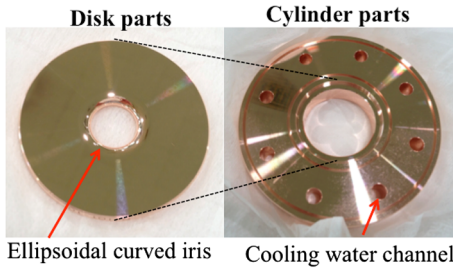
FIG. 4.   Disk (left) and the cylinder (right) of the accelerating cell.

FIG. 5.   Dispersion curves of the test cavities.

cross-sectional shape of the iris. (ii) Check the rf properties of the accelerating structure, such as normalized group velocity, quality factor, and shunt impedance. Three test cavities were machined with different dimensions; their iris diameters (2a) are 15.938 mm (type 1), 14.003 mm (type 2), and 12.106 mm (type 3). These dimensions correspond to the uppermost, midmost, and lowermost iris parts of the accelerating structure, respectively. Figure 4 shows photographs of the disk and cylinder parts that constitute the accelerating structure. The disk surfaces as well as the insides of the cylinder and the ellipsoidal shape of the iris were provided with a mirrorlike finish using an ultraprecision lathe in order to mitigate any concentration of the electric field. After machining, the surface roughness was measured using a three-dimensional shape measurement instrument and a surface roughness meter. The actual ellipsoidal shape of the iris considerably overlapped with the ideal ellipsoidal shape within 10 μm. The surface roughness of the disk and cylinder parts was around 0.06 μm, while that of the iris with the ellipsoidal shape was around 0.11 μm. Even though the ellipsoidal shape is not ideal the maximum dimensional difference from the ideal shape is 4.7 μm, which is significantly small for our purpose. We cannot show the actual graph data here, because the data include the manufacturing know-how of MHI.

B. Low-power rf test of the nine-cell test cavities

We checked whether the designed rf parameters of the C-band accelerating structure were realized using the test cavities, as follows. This check was also conducted to show the reliability of our accelerating structure design and whether a mass production process of the structure was possible from the trial manufacture stage. The resonant frequency and the quality factor of the TM01 $- 2\pi/3$ mode were measured using the test cavities. The quality factor of the test cavities was estimated from the loaded quality factor, and the coupling coefficient of the accelerating mode was measured by the network analyzer. Figure 5 shows the dispersion curve of the three types of test cavities. The numerically fitted curves in Fig. 5 were obtained using the following formula:
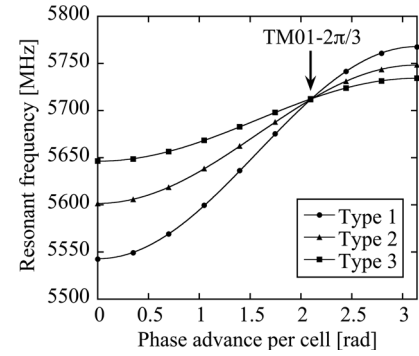
$$f = m_1 - m_2 \cos(\theta), \tag{3}$$

where f is the resonant frequency, m_1, m_2 are the proportionality factors related to the group velocity v_g, and θ is the phase advance per cell. The term m_2 denotes the differential coefficient of v_g. The v_g values of the individual cavities are obtained from the dispersion curves using the following formulas:

$$\frac{v_g}{c} = \frac{2\pi d}{c}\frac{df}{d\theta} = \frac{2\pi d m_2 \sin(\theta)}{c}, \tag{4}$$

where d is the cell spacing and c is the velocity of light [7]. Using the process described above, we obtained the v_g values of the test cavities. Table II lists the result of low-level rf measurements to characterize the rf performance of the test cavities. The v_g values of the test cavities are nearly consistent with our designed values, showing errors within 0.5 MHz. The quality factors are 82%–90% of the ideal cavity values. The discrepancies in the values are explained by the electrical contact losses and wall losses of the end plates of the test cavity. The measured v_g values are also consistent with the design values.

To estimate the shunt impedance of the test cavities, we measured the electric field distribution along the test cavities using the bead-pull perturbation method. The perturbing object was a sphere made of aluminum, having a diameter of 2 mm. Figure 6 shows the frequency change

TABLE II.   Measured results of the nine-cell test cavities. The designed values are stated in parentheses.

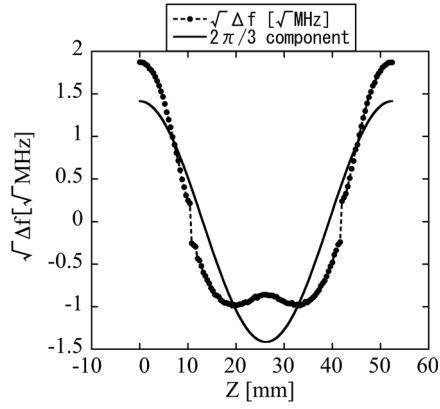|	Type 1	Type 2	Type 3
2a [mm] (30 °C vacuum)	15.938	14.003	12.106
2b [mm] (30 °C vacuum)	43.157	42.451	41.834
Resonant frequency [MHz]	5712.145	5712.084	5711.974
Quality factor	7400	8055	7940
	(8970)	(8910)	(8862)
Average group	0.0356	0.0231	0.0139
Velocity	(0.0346)	(0.0226)	(0.0135)

FIG. 6.   Change in frequency, i.e., Δf (acceleration-field pattern) as a function of the position of the bead and the $TM01 - 2\pi/3$-mode acceleration-field pattern reconstructed from the Δf data. The dashed line with the solid circles represents the on-axis acceleration electric-field pattern measured by the bead-pull perturbation method; the solid black curve is the reconstructed $TM01 - 2\pi/3$ accelerating mode.
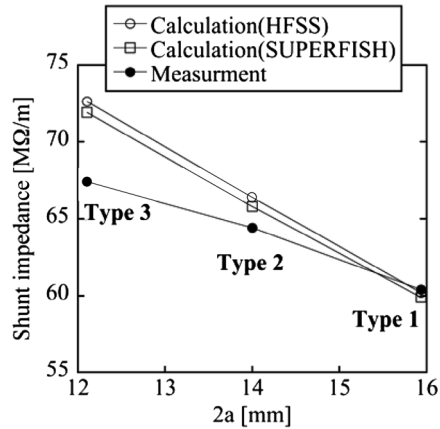

FIG. 7.   Shunt impedances along the accelerating cells of the three test cavities. The solid circles denote the measurement results. The open circles and open squares denote the calculated results obtained by HFSS [24] and SUPERFISH [27], respectively.

(Δf) as a function of the position of the bead moved along the center axis of the cavity. The Δf curve corresponds to an electric-field pattern including the fundamental mode and its space harmonics. Fourier analysis reconstructs the

acceleration-field pattern of the $TM01 - 2\pi/3$ mode into the fundamental mode from the Δf data. The shunt impedance, R_{sh}, of the cavities derived from the Δf data is expressed by

$$R_{sh} = \frac{|\Delta f| QL}{4\pi^2 \epsilon a_0^3 f_0^2},\tag{5}$$

where L is the length of the test cavity, ϵ is the dielectric constant of the perturbing object, a_0 is the radius of the perturbing object ($a_0 = 1$ mm) and f_0 is the resonant frequency of the cavity [26]. Figure 7 shows the shunt impedance of the three types of test cavities. The solid circles in Fig. 7 denote the measurement results; the open circles and open squares denote the results of calculations using the simulation codes of HFSS [24] and SUPERFISH [27], respectively. In the measurement, the average shunt impedance of the cavities was 64 MΩ/m, which corresponds to 97% of the calculated value. The measured value of the shunt impedance is sufficient to attain the required high-acceleration gradient of the structure.

IV. FABRICATION AND PHASE ADJUSTMENT OF THE 1.8 M ACCELERATING STRUCTURE

A 1.8-m-long accelerating structure was built on the basis of the above-mentioned experimental results obtained using the test cavities, as shown in Fig. 1. Copper blocks were used for the accelerating structure [class 1 oxygen-free copper treated with a hot isostatic pressing (HIP) process]. After all the disks and cylinder parts were machined, they were vertically stacked on a long V-block stage and brazed in a vacuum furnace. Then, a vacuum leak test and a hydraulic pressure resistance test were conducted to check for any vacuum leakage from the cell and the coupler as well as any water leakage from the cooling water channels.

To adjust the phase difference between the neighboring cells of the 1.8-m-long accelerating structure, the nodal shift method was used to measure the phase shift at each cell, and the dimpling method was adopted to tune the cell surface [20]. Finally, a nonresonant bead-pull perturbation method [28,29] was used to measure the electric field distribution and the cell frequency distributions along the cavity axis. Figure 8 shows
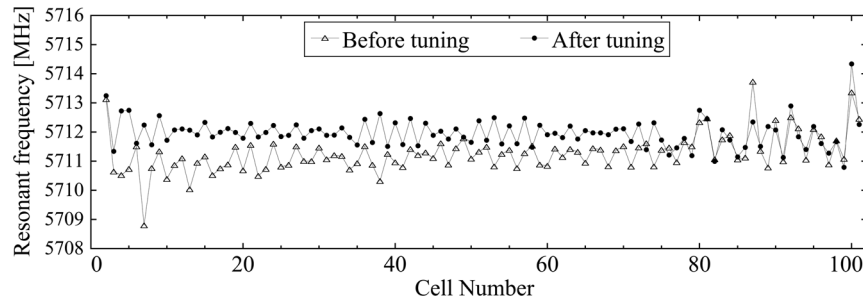

FIG. 8.   Resonant frequency distribution along the individual accelerating cells before and after dimpling tuning. The curve with open triangles represents the result before tuning, and the curve with solid circles represents the result after tuning.
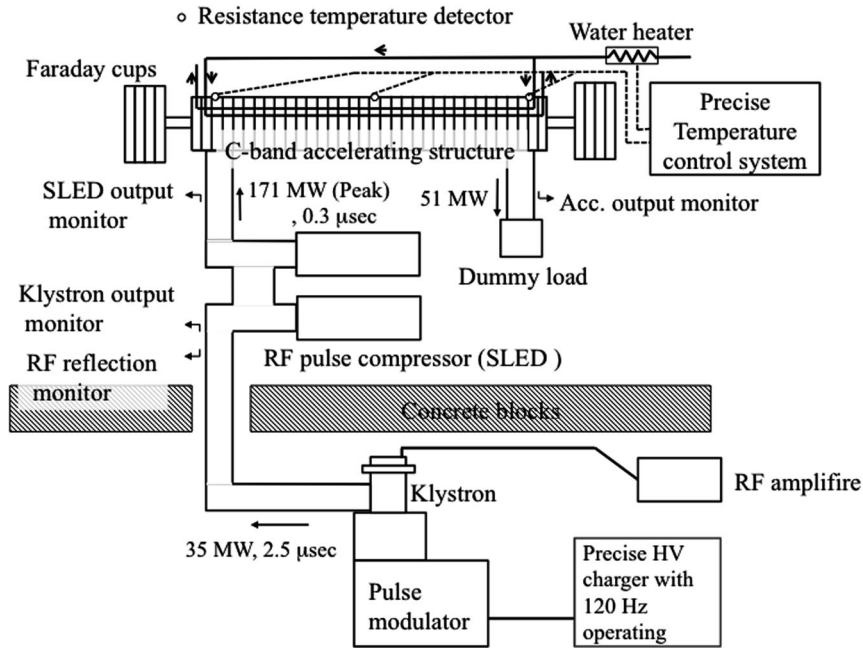
FIG. 9.   Schematic diagram of the experimental setup for the high-power rf test of the accelerating structure.

the distributions of the individual cell frequencies of the structure before and after tuning by the dimpling method. Tuning using the nodal shift and bead-pull perturbation data was performed to adjust the cell frequencies to 5712 MHz by pushing the cell walls through tuning holes. However, the resonant frequencies of some accelerating cells exceeded 5712 MHz after brazing. Pulling the cell wall lowered these resonant frequencies. Finally, the tuning nearly adjusted the resonant frequency distribution along the accelerating structure to within ±500 kHz from 5712 MHz, as shown in Fig. 8. The right side of Table I summarizes the performance achieved after tuning. We could obtain good results compared with the design parameters listed in Table I.

V. HIGH-POWER RF TEST OF THE *C*-BAND STRUCTURE

To evaluate the high-gradient performance of the structure, we performed a high-power rf test. We considered evaluating the following items in the high-power rf test.

1. The mitigation of the electric-field intensity on the surface of the ellipsoidal curved iris should be evaluated by measurements of the finally attained maximum acceleration gradient of the structure.

2. The dark current emitted from the inner surface of the structure should be measured to evaluate the inner surface roughness of the accelerating structure via measurement of the field enhancement factor β [30].

3. Operation stability under the high-acceleration-gradient condition should be checked by measuring the breakdown rate of the accelerating structure, which is related to 2.

4. Our designed heat-dissipation value of the structure under the designed operation condition should be evaluated. Figure 9 shows a schematic diagram of the experimental setup of the high-power test for the accelerating structure. The configurations of the experimental instruments and the individual high-power rf components for the test, such as the waveguides and the rf-pulse compressor, namely the SLAC energy doubler (SLED) [31], are nearly the same as those of SACLA. The accelerating structure and SLED are installed in a test bunker surrounded by concrete blocks used as a radiation shield.

Figure 10 shows the rf waveforms under rf conditioning. The klystron output rf power and the rf-pulse width are 35 MW and 2.5 μs, respectively. Because the SLED connected to the waveguide of the klystron multiplies its
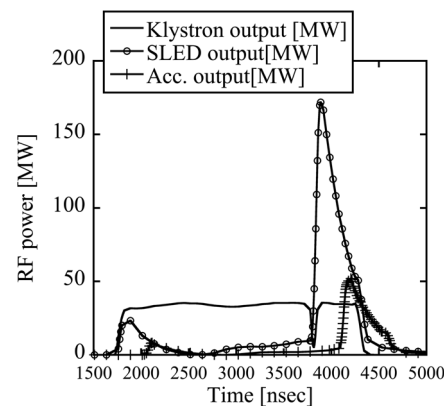

FIG. 10.   Waveforms of the klystron output (solid line), the SLED output (open circle), and the output after passing through the accelerating structure (plus sign).

output rf power by a factor of around 5, the peak power and the rf-pulse width of the SLED output become 171 MW and 0.5 μs, respectively. The output rf pulse of SLED is fed into the input coupler of the accelerating structure. When the rf pulse passes though the accelerating structure, the peak rf power gradually decreases to 51 MW at the output coupler owing to the wall loss of the structure. We calculated the acceleration gradient of the accelerating structure by Eq. (1), using the shunt impedance, R_{sh}, and the attenuation constant, τ. Our low-power rf measurements were obtained using these values. Here, the measured values of R_{sh} and τ are 64 MΩ/m and 0.54, respectively. The acceleration gradient calculated from the rf waveform data at the input coupler reaches 50.1 MV/m.

To measure the amount of dark current emitted from the structure, we observed electron charges captured using two Faraday cups that were installed at the two ends of the accelerating structure. Figure 11 shows the amount of dark current as a function of the acceleration gradient. The dark current decreases as the rf conditioning time increases. After 385 h, the amount of dark current becomes 150 pC/pulse at 50 MV/m. This dark current is small compared with that of the C-band choke-mode-type structure [32]. This result indirectly indicates that the dark current decreases proportionally with the intensity of the surface electric field. The field enhancement factor (β), which is an index of the surface roughness under a high electric field, is a suitable parameter for evaluating the dark current emission. From the dark current data given in Fig. 11, we can calculate the field enhancement factor, β by

$$\frac{d(\log_{10} \frac{I}{E_p^{2.5}})}{d(\frac{1}{E_p})} = -\frac{2.84 \times 10^9 \phi^{1.5}}{\beta}, \qquad (6)$$

where I is the amount of dark current, E_p is the surface electric field strength, and ϕ is the work function of copper

(4.5 eV) [30]. Finally, we obtained a β value that was between 73 and 79 during rf conditioning of the accelerating structure. According to Refs. [30,32–35], the β value is between 38 and 122 under a long operation time for 235–811 h. Our obtained β value is consistent with the values described in Refs. [30,32–35]. This fact indicates that the surface roughness of the ellipsoidal shape of the iris is sufficiently small for our purpose.

To measure the breakdown rate, the accelerating structure was continuously operated at the same acceleration gradient values for 24 h. The measurement was performed at 256 and 370 h after the start time of the rf conditioning. Figure 12 shows the breakdown rate per day of the accelerating structure as a function of the acceleration gradient. This rate finally decreased to acceptable values for practical operation. We operated the structure at an acceleration gradient of 42 MV/m; the breakdown rate with interlocked halts by electric discharges was once or less per day at 256 h after the conditioning started. Furthermore, the breakdown rate at 370 h and 50 MV/m decreased to around 40% of the breakdown rate at 256 h. The achieved breakdown rate of the structure was once or less per day at around 42 MV/m, which was the established acceleration gradient at SACLA. We can say that this rate is less than that of SACLA, because the new accelerating structure can operate at a higher acceleration gradient than SACLA while maintaining the same breakdown rate at SACLA. Furthermore, we compared the breakdown rate with those of the various accelerating structures described in Ref. [16] to analyze the breakdown behavior, as mentioned in the Introduction. We also checked whether the high-gradient characteristics of our developed structure are extensions of the characteristics of the ordinary accelerating structure. Figure 13 shows the breakdown rate per pulse as a function of the acceleration gradient. The unit of the breakdown rate is changed from count/day to bpp (breakdown per pulse). Here, the breakdown rate of the C-band structure at
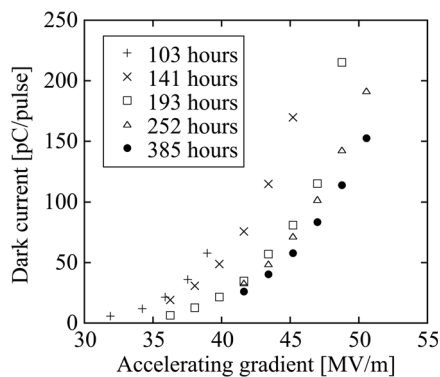

FIG. 11.   Dark current emissions dependent on the acceleration gradients as the conditioning time changes. The plus signs, open crosses, open squares, open triangles, and solid circles corresponding to conditioning times of 103, 141, 193, 252 and 385 h after the start of conditioning, respectively.
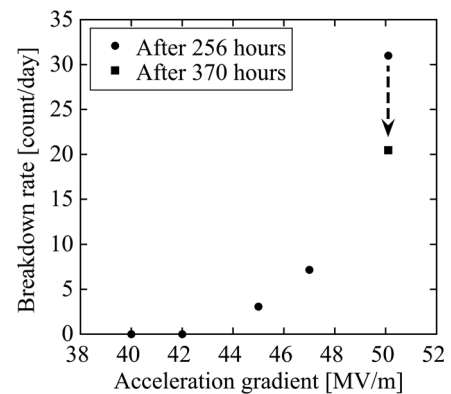

FIG. 12.   Breakdown rate per day as a function of the acceleration gradient. The solid circles and solid squares denote the breakdown rates at 256 and 370 h after the start of conditioning, respectively.
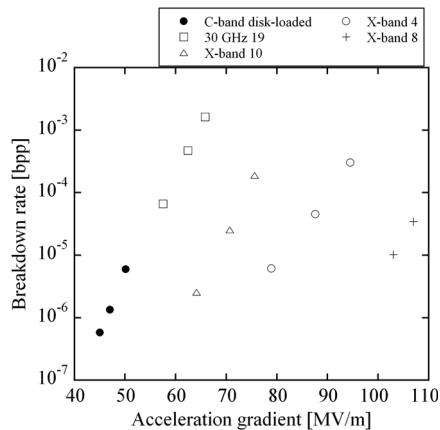
FIG. 13. Breakdown rate per pulse as a function of the acceleration gradient. The solid circles represent the case of the C-band disk-loaded-type accelerating structure, and the other markers represent the breakdown rates of the various structures in Ref. [16].

50 MV/m is 6.0×10^{-6} bpp. The relation between the acceleration gradient and the breakdown rate is given by

$$E_a^{30}/BDR = \text{const}, \qquad (7)$$

where E_a is the acceleration gradient of the accelerating structure. The breakdown rates satisfy the condition of Eq. (7); thus, they are consistent with the results of the Ref. [16].

To investigate the thermal characteristics of the accelerating structure, we measured the heat dissipation value under 120 pps operation via calorimetric analysis using the cooling-water temperature difference between the inlet and outlet of the accelerating structure. During the measurement, the temperature of the accelerating structure was maintained within $30 \pm 0.01\,^\circ\text{C}$ using a precise temperature control system. To measure the temperature of the accelerating structure, resistance temperature detectors are attached to the middle cell of the accelerating structure, as shown in Fig. 14(a). One of the measurement points (Point 1) is the bottom of a tuning hole (diameter, 1.5 mm; depth, 10 mm). Another point (Point 2) is the bottom of the tuning hole (diameter, 5 mm; depth, 35 mm). Figure 14(b) shows the temperature data at the points described in Fig. 14(a) and at the inlet and outlet of the cooling water when the acceleration gradient was 50 MV/m. Here, the temperature difference between the inlet and outlet cooling water is 3.5 K, and the heat dissipation value is 4.7 kW under an rf-pulse repetition rate of a 120 pps and an acceleration gradient of 50 MV/m. This heat dissipation value is consistent with the value calculated from the difference between the input and output rf powers. In addition, when the temperature control system stabilized the temperature at Point 1, the temperature at Point 2 was 0.5 K higher than that at Point 1, as shown in Fig. 14(b). This result is consistent with the model calculation of
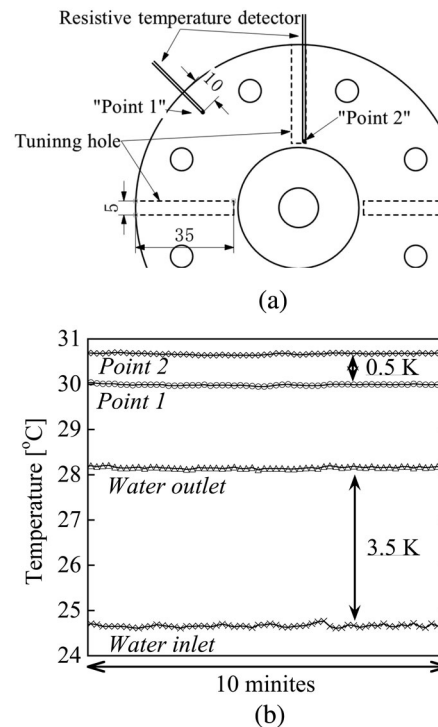

(a)

(b)

FIG. 14. (a) Schematic view of the measurement points where the resistive temperature detectors are located in the middle cell of the accelerating structure. (b) Temperature trends at "Point 1" and "Point 2" of the accelerating structure as well as the trends at the inlet and outlet of the cooling water when the acceleration gradient was 50 MV/m.

the accelerating cell, as shown in Fig. 3. Furthermore, even if the rf-pulse repetition rate is changed, the phase change of the rf pulse that passes through the accelerating structure is 1°. The reduction in the acceleration gradient by this phase change is quite small (around 0.02%) compared to our requirement. From the above-mentioned results, we believe that our cooling system design for the structure is optimum.

VI. ACCELERATION OF THE ELECTRON BEAM

Ten columns of the C-band accelerating structures were installed as the main accelerator of an extreme ultraviolet (EUV)-FEL beam line [36]. To measure the acceleration gradient of the C-band accelerating structure, we measured the beam energy at the magnetic chicane consisting of four bending magnets, which is placed after the six accelerator columns. The experimental setup for this measurement is shown in Fig. 15(a). When we measured the beam energy, the rf phase of two 1.776-m-long columns (these accelerator columns are driven by one high-power klystron) was changed. Figure 15(b) shows the energy of an electron beam accelerated with the two columns corresponding to one unit, as a function of their rf phase. The beam was finally accelerated up to 147 MeV with the crest phase. From the data, the acceleration gradient was calculated to
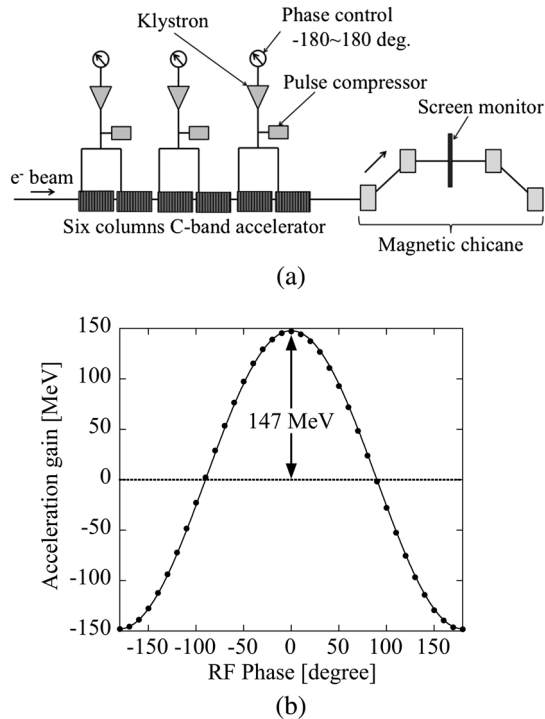
(a)

(b)

FIG. 15. (a) Schematic diagram of the *C*-band accelerator section in the EUV-FEL accelerator. (b) Acceleration energy gain of the two 1.8-m-long *C*-band accelerating structures as a function of the rf phase. The maximum acceleration energy gain is 147 MeV.

be 41.4 MV/m. This acceleration gradient is consistent with the calculation using the measured rf power and the shunt impedance, as well as τ of the structure using Eq. (1). From the observation, we conclude that the required performance of the *C*-band accelerating structure has been realized.

VII. SUMMARY

We developed a 1.8-m-long *C*-band disk-loaded-type accelerating structure that can be adopted with a high acceleration gradient of >50 MV/m and operated with a high rf-pulse repetition rate of up to 120 pps. A cross section with an ellipsoidal curvature around an iris aperture was employed to reduce the strength of the electric field on the iris surface. After machining the structure, the actual dimensions of the iris ellipsoidal shape were compared with the ideal dimensions. The geometrical shape of the iris considerably overlapped with the ideal ellipsoidal shape within 10 μm. This agreement indicates a considerable possibility of reducing the electric field. Furthermore, the rf parameters of the manufactured *C*-band accelerating structure were checked. They were nearly consistent with our designed parameters. Next, the optimum arrangement of the water-cooling channels around the cell of the accelerating structure was determined according to the design for adapting to 120-pps operation. In this case, the maximum designed temperature on the cell surface was 35.2 °C at an

average heat load of 3.8 kW, which was the designed heat dissipation value. A high-power rf test was performed to check the above-mentioned features of the accelerating structure. The results showed that the acceleration gradient of the structure reached 50.1 MV/m. As evidence of the mitigation of the electric field strength of the iris surface, we measured the dark current at the downstream side of the accelerating structure. The dark current was sufficiently small compared with that of the *C*-band choke-mode-type structure. This means that the surface electric field of the developed structure is less than that of the *C*-band choke-mode-type structure. The breakdown rate of the accelerating structure gradually decreased to acceptable values for our operation after a certain conditioning time. This rate was around once per hour at an acceleration gradient of 50 MV/m and an operational rf-pulse repetition rate of 120 pps. Furthermore, the breakdown rate of the *C*-band structure satisfied Eq. (7) and was consistent with the results presented in Ref. [16]. We confirmed that the high-acceleration gradient characteristics of our developed accelerating structures are extensions of the characteristics of the ordinary structure. These results indicate that the surface electric field strength decreases because of the ellipsoidal curvature of the iris. Furthermore, the temperature difference between two points [Fig. 14(a)] in the middle cell of the accelerating structure was consistent with the result of a thermal calculation of the cell model. The average heat dissipation value was 4.7 kW at operating conditions of 120 pps and 50 MV/m. The measured heat dissipation value was different from the above-mentioned designed value because of the difference in the assumed input rf power. When considering the difference the measured heat dissipation value was identical to the designed value. It agreed well with the above-mentioned heat dissipation value calculated from the rf powers difference between the input and output parts. These results showed that the structure could correspond with 120-pps operation. This structure was finally installed as the main accelerator of our EUV-FEL accelerator. Then, in electron-beam acceleration, the acceleration gradient reached 41.4 MV/m. The obtained acceleration gradient was in agreement with the result of the high-power rf test. From the above-mentioned facts, we can say that we succeeded in the development of a *C*-band disk-loaded-type accelerating structure showing the required performance to achieve a high acceleration gradient of >50 MV/m and an rf repetition rate of 120 pps. The *C*-band disk-loaded-type accelerating structure can be applied now to various electron accelerators involving reinforcement of the electron beam energy and reduced accelerator length.

their management and promotion. The authors would also like to thank the SACLA operator group for maintenance and regular monitoring of the rf test stand.

[1] P. Emma *et al.*, First lasing and operation of an angstrom-wavelength free-electron laser, Nat. Photonics **4**, 641 (2010).

[2] T. Ishikawa *et al.*, A compact X-ray free-electron laser emitting in the sub-angstrom region, Nat. Photonics **6**, 540 (2012).

[3] M. Altarelli *et al.*, DESY Report No. 2006–097, 2007.

[4] R. Ganter, SwissFEL Conceptual Design Report, Villigen, 2011, V19.

[5] J. H. Han, H. S. Kang, and I. S. Ko, Status of the PAL-XFEL Project, in *Proceedings of the 3rd International Particle Accelerator Conference, New Orleans, LA, 2012* (IEEE, Piscataway, NJ, 2012).

[6] T. Bizen, T. Tanaka, Y. Asano, D. E. Kim, J. S. Bak, H. S. Lee, and H. Kitamura, Demagnetization of the undulator magnets irradiated high energy electrons, Nucl. Instrum. Methods Phys. Res., Sect. A **467–468**, 185 (2001).

[7] R. B. Neal *et al.*, *The Stanford Two-miles Accelerator* (W.A. Benjamin, Inc., New York, 1968).

[8] S. Reiche *et al.*, Status of the SwissFEL facility at the Paul Scherrer Institute, in *Proceedings of 33rd International Free Electron Laser Conference, Shanghai, China*, 2011.

[9] T. Hara *et al.*, Time-interleaved multienergy acceleration for an x-ray free-electron laser facility, Phys. Rev. ST Accel. Beams **16**, 080701 (2013).

[10] T. Shintake *et al.*, The choke mode cavity, Jpn. J. Appl. Phys. **31**, L1567 (1992).

[11] T. Inagaki, C. Kondo, H. Maesaka, T. Ohshima, Y. Otake, T. Sakurai, K. Shirasawa, and T. Shintake, High gradient C-band linac for a compact x-ray free-electron laser facility, Phys. Rev. ST Accel. Beams **17**, 080702 (2014).

[12] T. Kamitani *et al.*, Status of C-band accelerator module in the KEKB injector LINAC, in *Proceedings of the 22nd Particle Accelerator Conference, PAC-2007, Albuquerque, NM* (IEEE, New York, 2007).

[13] D. Alesini *et al.*, The C-band accelerating structure for SPARC photoinjector energy upgrade, J. Instrum. **8**, P05004 (2013).

[14] R. Zennaro *et al.*, Design, construction and power conditioning of the first C-band test accelerating structure for SwissFEL, in *Proceedings of 26th Linear Accelerator Conference, Tel Aviv, Israel*, 2012.

[15] W. Fang, D. Tong, Q. Gu, and Z. Zhao, Design and experimental study of a C-band travelling-wave accelerating structure, Chin. Sci. Bull. **56**, 18 (2011).

[16] A. Grudiev, S. Calatroni, and W. Wuensch, New local field quantity describing the high gradient limit of accelerating structures, Phys. Rev. ST Accel. Beams **12**, 102001 (2009).

[17] T. Taniuchi *et al.*, Development of low dark current accelerating structure at SPring-8 Linac, in *Proceedings*

[18] *of 6th Annual Meeting of Particle Accelerator Society in Japan, Tokai, Ibaragi, Japan* (PASJ, Japan, 2009).

[18] V. A. Dolgashev *et al.*, Report No. SLAC-PUB-10175, 2003.

[19] R. H. Miller *et al.*, A damped detuned structure for the Next Linear Collider, in *Proceedings of 18th Linear Accelerator Conference, Geneva, Switzerland*, 1996, p. 644.

[20] W. J. Gallagher, SLAC-Project M Report No. M-205, 1960.

[21] V. F. Khan, A. D'Elia, R. M. Jones, A. Grudiev, W. Wuensch, G. Riddone, and V. Soldatov, Wakefield and surface electromagnetic field optimization of manifold damped accelerating structures for CLIC, Nucl. Instrum. Methods Phys. Res., Sect. A **657**, 131 (2011).

[22] F. Wang, C. Adolphsen, and C. Nantista, Performance limiting effects in X-band accelerators, Phys. Rev. ST Accel. Beams **14**, 010401 (2011).

[23] H. Tanaka *et al.*, Bunch length variation and timing jitter caused by RF system instability in XFELSPring-8, in *Proceedings of 4th Annual Meeting of Particle Accelerator Society in Japan, Wako, Saitama, Japan* (PASJ, Japan, 2007).

[24] http://ansys.com.

[25] T. Hasegawa *et al.*, Status of a precise temperature-regulation system for the C-band accelerator at XFEL/SPring-8, in *Proceedings of the International Particle Accelerator Conference, Kyoto, Japan* (ICR, Kyoto, 2010).

[26] E. L. Ginzton, *Microwave Measurements* (McGraw-Hill Book Company, Inc., New York, 1957).

[27] http://laacg.lanl.gov/laacg.

[28] T. Khabiboulline *et al.*, Internal Report No. DESY M-95-02, 1995.

[29] H. Ego, H. Maesaka, T. Sakurai, Y. Otake, T. Hashirano, and S. Miura, Transverse C-band deflecting structure for longitudinal electron-bunch-diagnosis in XFEL "SACLA", Nucl. Instrum. Methods Phys. Res., Sect. A **795**, 381 (2015).

[30] G. A. Loew *et al.*, Report No. SLAC-PUB-4647, 1988.

[31] Z. D. Farkas *et al.*, Report No. SLAC-PUB-1453, 1974.

[32] T. Sakurai *et al.*, High power RF test on the C-band RF components of 8 GeV accelerator for XFEL/SPring-8, in *Proceedings of the 23rd Particle Accelerator Conference, Vancouver, Canada, 2009* (TRIUMF, Canada, 2009).

[33] Y. Igarashi *et al.*, KEK Report No. 2003–9, 2004.

[34] T. Inagaki *et al.*, High gradient test on the C-band choke-mode type accelerating structure, in *Proceedings of 1st Annual Meeting of Particle Accelerator Society in Japan, Funahashi, Chiba, Japan* (PASJ, Japan, 2004).

[35] T. Taniuchi *et al.*, High power test of low dark current accelerating structure, High power test of low dark current accelerating structure, in *Proceedings of the 8th Annual Meeting of Particle Accelerator Society of Japan, Tsukuba, Japan* (PASJ, Japan, 2011).

[36] Y. Otake *et al.*, Relocation and improvement status of the SCSS test accelerator to provide dual FEL drivers at SACLA, in *Proceedings of 6th International Particle accelerator conference, Richmond, Virginia, USA*, 2010.